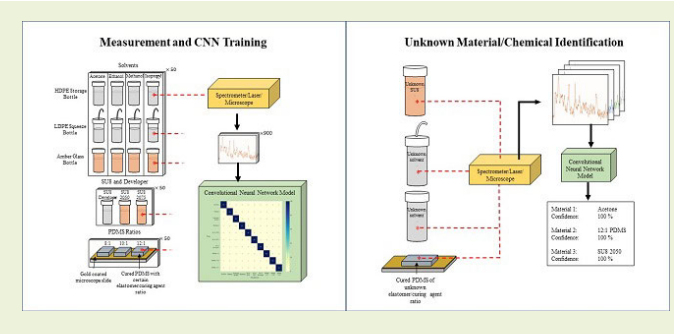


Identification of Unknown Nanofabrication Chemicals Using Raman Spectroscopy and Deep Learning

Nicholas Theobald[®], Donald Ledvina, Kaitlyn Kukula, Sofia Maines[®], Kathryn Hasz, Markus Raschke, Jerry Crawford, Jeff Jessing, and Yivan Li

Abstract—Raman spectroscopy is a common identification and analysis technique used in research and manufacturing industries. This study investigates the use of Raman spectroscopy and deep learning techniques for identifying various nanofabrication chemicals. Four solvents and SU-8 developer were identified inside common chemical storage and distribution containers. The containers attenuated the spectra and contributed varying amounts of background fluorescence, making manual identification difficult. Two varieties of SU-8 photoresist were differentiated inside amber glass jars, and cured samples of three ratios of polydimethylsiloxane (PDMS) were differentiated using Raman microscopy. The neural network accurately identified



the nanofabrication chemicals 100% of the time, without additional preprocessing. This investigation demonstrates the use of Raman spectroscopy and neural networks for the identification of nanofabrication chemicals and makes recommendations for use in other challenging identification applications.

Index Terms—Convolutional neural nets, deep learning, machine learning, nanofabrication, Raman spectroscopy.

I. INTRODUCTION

R AMAN spectroscopy is a nondestructive, contact-free, chemical identification, and analysis technique often used in forensics, biology, materials science, pharmaceuticals, and nanotechnology [1]. Materials can be identified based on a set of Raman peaks and other spectral features can be related to the crystallinity, uniformity, temperature, and stress inside of a material [2]. Pairing Raman spectroscopy with

Manuscript received 3 February 2023; accepted 9 February 2023. Date of publication 2 March 2023; date of current version 31 March 2023. This work was supported in part by the National Science Foundations NSF STROBE under Grant #1548924, in part by the NSF PREM under Grant #1827847, and in part by the NSF REU under Grant #1757953. The associate editor coordinating the review of this article and approving it for publication was Dr. Sanket Goel. (Corresponding author: Yiyan Li.)

Nicholas Theobald, Kaitlyn Kukula, Jerry Crawford, Jeff Jessing, and Yiyan Li are with the Department of Physics and Engineering, Fort Lewis College, Durango, CO 81301 USA (e-mail: yli@fortlewis.edu).

Donald Ledvina is with the Bayfield High School, Bayfield, CO 81122 USA.

Sofia Maines is with the Durango High School, Durango, CO 81301 USA.

Kathryn Hasz and Markus Raschke are with the Department of Physics, University of Colorado Boulder, Boulder, CO 80309 USA.

This article has supplementary downloadable material available at https://doi.org/10.1109/JSEN.2023.3249668, provided by the authors. Digital Object Identifier 10.1109/JSEN.2023.3249668

optical microscopy allows for the analysis of micrometerscale samples and structures, making Raman spectroscopy a popular technique for analyzing micro-electromechanical systems (MEMS) and semiconductor devices [2], [3]. Due to its nondestructive, contact-free nature, it has recently become a popular method for identifying materials in situ, with minimal preprocessing. Portable Raman spectrometers have also been developed to detect pollutants in environmental samples [4], [5], to remotely detect explosive materials [6], [7], to monitor SU-8 photoresist exposure [3], to identify biological materials through the container walls, both in vivo and in vitro [1], [8], and to authenticate olive oil inside the original container [9]. Although the portable Raman systems hold promise as an easy-to-use, quick, and fielddeployable instrument for the evaluation of a variety of materials, the accuracy achieved by the embedded pattern recognition software and hardware is not always 100% [10]. If the container or substrate of the substance changes, the acquired signal could be unidentifiable by a general-purpose handheld Raman system. It is challenging to customize the software of a commercial product, work with a large dataset, and manually identify each material [11], [12], [13]. For this reason, machine learning techniques are gaining popularity for automating the spectral identification

1558-1748 © 2023 IEEE. Personal use is permitted, but republication/redistribution requires IEEE permission. See https://www.ieee.org/publications/rights/index.html for more information.

process. Some of the most common algorithms used to identify materials include random forest, support vector machine, k-nearest neighbors, multilayer perceptron, fully connected neural networks, convolutional neural networks (CNNs), and principal component analysis [12], [14], and most of these libraries are open-source.

Misidentifying laboratory chemicals and materials can lead to delays and potentially result in dangerous situations. The labeling on chemical storage containers can become damaged over time from exposure to chemicals in the environment. Mediating this risk is especially important for labs that reuse chemicals and regularly transfer them to new containers. Instrument and human error can also lead to mistakes in procedures, resulting in products that do not perform as expected or cannot be used for subsequent processes.

This study proposes the use of Raman spectroscopy and deep learning techniques to identify unknown solvents and materials in the context of a nanofabrication laboratory. The entire script used for this study and the user instruction are made open-source (see Supplementary Materials). The adoption of this technique would allow labs to quickly verify their chemicals in the event of a damaged label or a mistake in processing. Under normal laboratory conditions, identifying various chemicals and materials using Raman spectroscopy is trivial. However, through-wall identification requires the excitation laser and Raman signal to pass through the walls of the container. The container contributes its own Raman peaks and fluorescence and significantly attenuates the characteristic Raman peaks of the chemical. There is also a lack of documentation using Raman spectroscopy to differentiate varieties of uncured SU-8 photoresist. SU-8 photoresist is a photocuring epoxy resin used to make micrometer-scale structures. The thickness of these structures can be partly controlled by using different viscosities. The resist can only be opened under certain lighting and should not be opened outside of a fume hood. Bottle identification could allow labs to easily identify viscosities of SU-8 photoresist. Bottle identification of SU-8 developer would also be beneficial. There is also a lack of documentation identifying the ratio of elastomer and curing agent in cured polydimethylsiloxane (PDMS). PDMS is a flexible and chemically inert silicone rubber that is often used in microfluidic chip fabrication. The elastic modulus of PDMS is important for ease of fabrication and the functionality of the microfluidic device. Once the two parts (elastomer and curing agent) have been mixed, there are a few nondestructive options for ensuring that the correct ratio was used. However, there are subtle shifts in the spectra. Nanofabrication labs could use this technique to differentiate between similar viscosities of SU-8 photoresist and to verify the ratio of elastomer and curing agent used in cured PDMS microfluidic chips.

To demonstrate the capability of our proposed technique, three experiments were performed. The first experiment identified four common nanofabrication solvents inside application-relevant containers. The chemicals include acetone, ethanol, isopropyl alcohol, and methanol. The solvents were identified inside amber glass jars, low-density polyethylene (LDPE) squeeze bottles, and high-density polyethylene (HDPE) jars. An SU-8 developer also should not be opened outside of a



Fig. 1. Common storage containers: (a)–(c) LDPE squeeze bottles, (d) HDPE jar, and (e) amber glass jar.

fume hood. The amber glass jars are similar to the glass containers used for shipping and storage. They are also used to store light-sensitive materials, such as SU-8 photoresist, since they block certain wavelengths of light. The LDPE squeeze bottles are typically used for administering small amounts of solvent. The HDPE containers are often used for long-term storage and are typical for storing SU-8 developer. The second experiment differentiated two varieties of SU-8 photoresist: SU-8 2050 and SU-8 2075. These were identified inside amber glass jars. The last experiment differentiated cured samples of PDMS that used three different ratios of elastomer and curing agent: 8:1, 10:1, and 12:1. Due to the weak Raman scattering of PDMS, these samples were measured on gold-coated microscope slides. Surface-enhanced Raman spectroscopy (SERS), enabled by the gold-coated slides, improved the performance of the PDMS measurements. These slides are often used for detecting weak samples and even single molecules [11]. Due to the SERS effect, the intensity of the Raman peaks was increased and further distinguished the spectra from background noise. These slides also contributed minimal background fluorescence, in contrast to uncoated glass slides.

The CNN identified all samples with no error. This result is expected for the solvents in the LDPE squeeze bottles and the SU-8 photoresist, due to signal strength and the difference between the spectra. The advantage of the neural network became especially apparent for the HDPE jars, where even the main characteristic peaks were difficult to identify in individual spectra. For the same reason, the neural network was necessary for differentiating the three ratios of PDMS.

II. METHODS

A. Raman Measurements

Raman measurements were performed using a Raman-HR-TEC-785 Raman spectrometer from StellarNet Inc. The spectrometer came equipped with a 1200 lines/mm diffraction grating providing a resolution of 4 cm⁻¹ with a spectral range of 200–2750 cm⁻¹. The detector was a 2048-pixel Sony ILX CCD detector, cooled to –15 °C by a single-stage thermoelectric cooler. The detector had a signal-to-noise ratio of 1000:1. The system was fiber coupled to a Raman probe

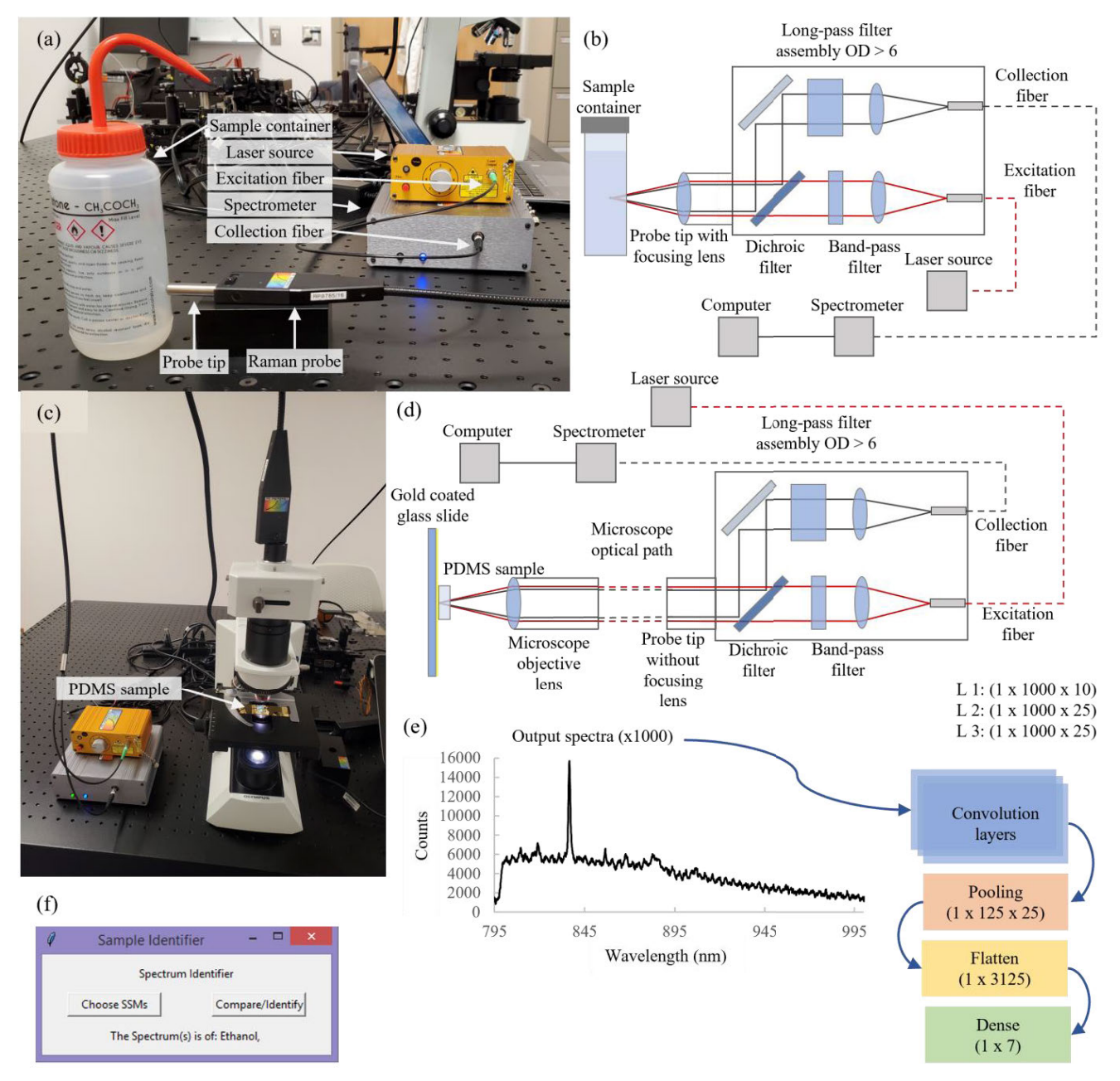


Fig. 2. System layout for container and glass slide measurements: (a) experimental setup for container measurements, (b) system diagram for container measurements, (c) experimental setup for glass slide measurements, (d) system diagram for glass slide measurements, (e) model diagram of the neural network, and (f) GUI for data loading and classification.

that had a working distance of 4.5 mm, allowing the beam to focus inside the containers. The probe was used to perform measurements of the solvents, SU-8 developer, and SU-8 photoresist. The containers shown in Fig. 1 were filled with each solvent. Fig. 1(a)–(c) shows the LDPE squeeze bottles for methanol, acetone, and isopropyl alcohol, respectively. Fig. 1(d) shows the HDPE jar and Fig. 1(e) shows the amber glass jar.

The experimental setup for container measurements is shown in Fig. 2(a). The system diagram for container measurements is shown in Fig. 2(b). For amber glass jars and LDPE squeeze bottles, the laser power and integration time were set to 330 mW and 15 s, respectively. To account for

signal attenuation, from the HDPE jars, the laser power and integration time were set to 450 mW and 30 s, respectively. Fifty measurements were collected at ten locations along the perimeter of the containers using the Raman probe. This methodology was repeated for the two viscosities of SU-8 photoresist in amber glass jars and for the SU-8 developer in HDPE jars. The SU-8 developer came in an HDPE jar with slightly thinner walls than those used for the solvents. To account for this, the integration time was reduced to 15 s. A 2-mm-thick layer of each PDMS ratio (8:1, 10:1, and 12:1) was poured onto three separate glass microscope slides. The samples were cured for 24 h and then were transferred to a microscope slide coated with a 100-nm-thick layer of gold,

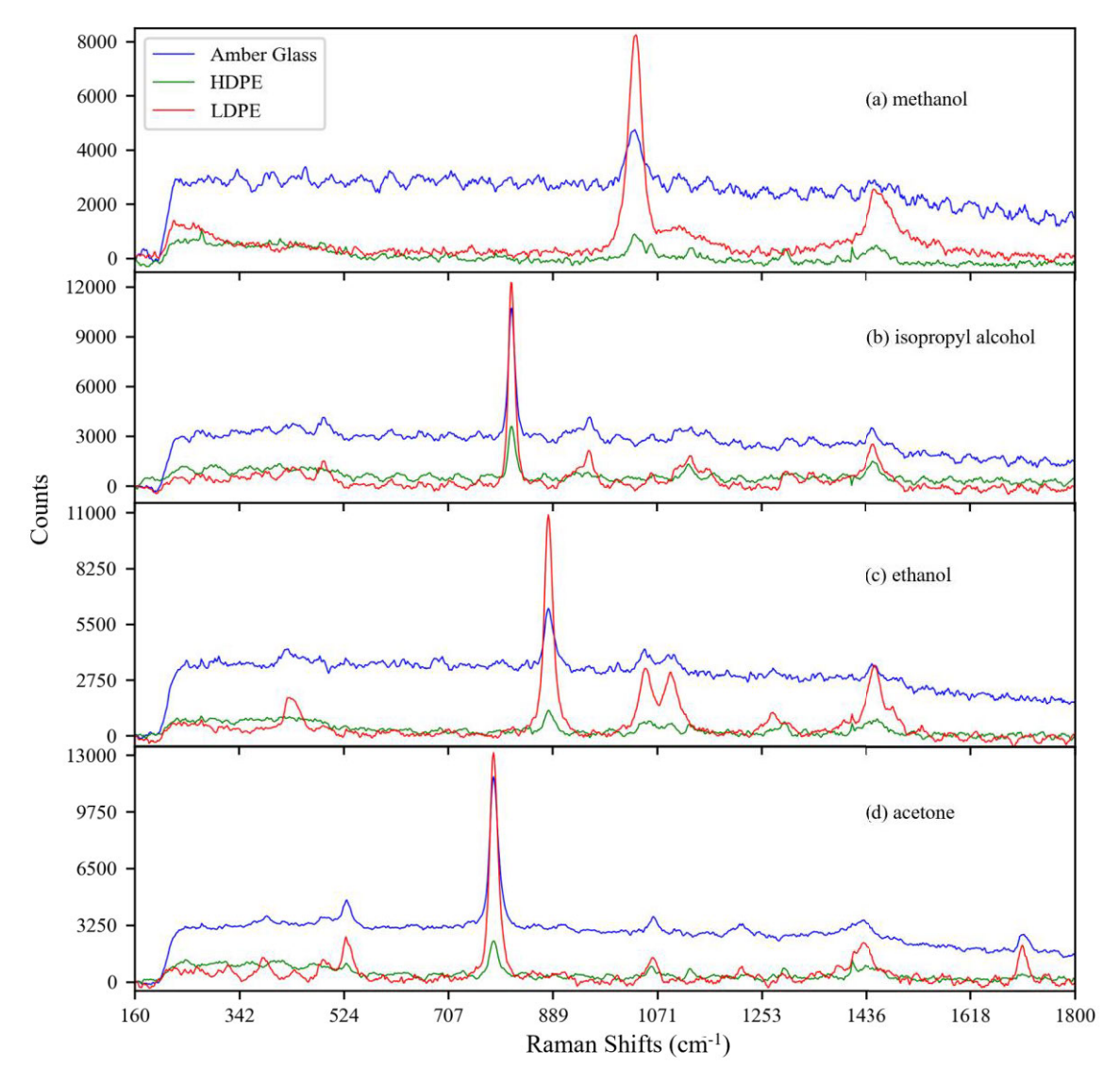


Fig. 3. Averaged and offset corrected Raman spectra of the four solvents in each container: (a) methanol, (b) isopropyl alcohol, (c) ethanol, and (d) acetone.

purchased from Platypus Technologies. The PDMS samples were then measured using the Raman probe coupled with an Olympus CX31 microscope purchased from Stellarnet. A $10\times$ objective was used to focus on the underside of the PDMS samples, avoiding any air bubbles in the PDMS. The integration time and the laser power were set to 10~s and 330~mW, respectively. Fifty measurements were collected with ten random locations on each sample to account for differences in sample thickness.

B. Neural Network and Spectra Identification

The four-layer CNN, outlined in the work by Kukula et al. [15], was adapted to accept the dataset generated in this study. This code allows for pretraining, testing, and fine-tuning of provided datasets. A diagram of the network can be seen in Fig. 2(e). It consists of three consecutive convolutional layers, followed by one pooling layer, one flattened layer, and a final dense classification layer. This yields a total network depth of four layers. The

convolutional kernel size was $5 \times 5 \times 5$ and the filter size was $10 \times 25 \times 25$. The batch size for pretraining and fine-tuning was 100 and 12, respectively. The number of epochs for both pretraining and fine-tuning was 30. The learning rate for both pretraining and fine-tuning was 0.001.

Python was used to individually normalize the data and split it into arrays, an *x*-array for data arrays and a *y*-array for classification arrays. An array for each category per material was created. The final *x* array used in classification was created by concatenating each category together.

The CNN was first trained on 38 random labeled spectra of each sample, with a vector output of possibilities across the solvent types. Fine-tuning and testing were conducted on six random spectra allowing for calculations of classification accuracies. These datasets were then combined with the datasets from the other containers, for each solvent. The final model dataset for each solvent was composed of 114 spectra for pretraining, 18 spectra for fine-tuning, and 18 spectra for testing. The datasets for the other samples were broken down

similarly: 38 spectra for pretraining, six spectra for fine-tuning, and six spectra for testing. This model also allows for manual hyperparameter tuning.

For tracking model accuracy, a confusion matrix was used. Model efficiency was studied by plotting the model's performance in relation to the number of epochs, allowing for the model to be manually tuned for time efficiency.

The network also produced an exportable model for use on other devices. A graphical user interface (GUI) was created to load unknown spectra and display the predicted classification, as shown in Fig. 2(f). The GUI directly loads the selected spectra from the spectrometer (referred to as.SSM files), compares them to the exported model, and then displays the classification that had the highest similarity to the unknown spectrum. The code for data preprocessing, the neural network, and the GUI are shown in the Supplementary Document.

III. RESULTS

The first experiment measured the spectra of the four solvents inside each of the three types of containers. This allowed the model to account for the fluorescence and attenuation caused by the containers. A total of 150 spectra were collected for each solvent, with 50 spectra per container. The measurements were broken into ten locations along the perimeter of the containers, to account for variations in wall thickness. The spectra were corrected for any initial offset and then averaged, as shown in Fig. 3(a)–(d). In these figures, the offset caused by the material of the containers is clearly shown. The amber glass jars contribute less overall attenuation than the HDPE jars but obscure the Raman peaks with additional noise. However, all of the characteristic peaks are present in these spectra: 798 cm⁻¹ for acetone; 883 cm⁻¹ for ethanol; 820 cm⁻¹ for isopropyl alcohol; and 1035 cm⁻¹ for methanol.

To determine the network's ability to differentiate varieties of the same substance, the last experiment measured two viscosities of SU-8 photoresist and three ratios of PDMS. Both varieties of SU-8 were tested inside amber glass jars. Fifty spectra were collected for both viscosities, measured at ten random locations along the perimeter of the jars. The offset-corrected and averaged spectra from the two SU-8 viscosities are shown in Fig. 4. The spectra of SU-8 2050 had greater intensities than that of SU-8 2075. A number of the strongest characteristic peaks are shown in both spectra: 900, 1253, and 1816 cm⁻¹.

Cured samples of the three PDMS ratios were measured on gold-coated glass microscope slides. Fifty spectra were collected for each ratio at ten random locations on the samples. The averaged and offset corrected spectra from each of the mixtures are shown in Fig. 5. All three ratios show characteristic peaks (472, 607, and 692 cm⁻¹) that are indistinguishable by eye.

To build a more complete model, the SU-8 developer was also measured. The developer was tested inside an HDPE container that had slightly thinner walls than those used for the solvents. For this reason, an integration time of 15 s was used. As with the solvents, 50 spectra were collected at ten random locations along the perimeter of the container. The

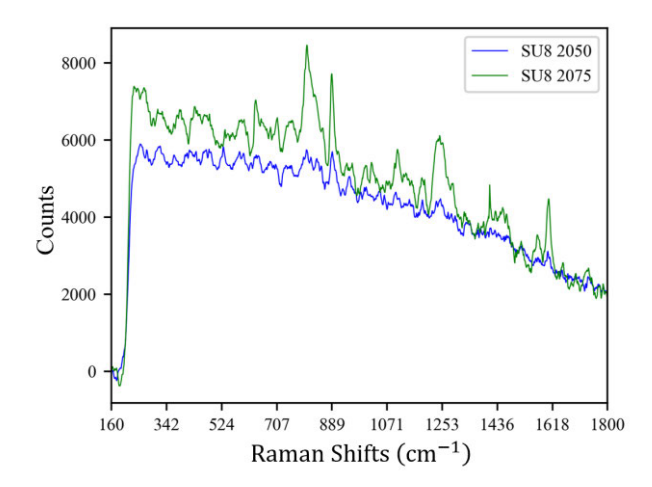


Fig. 4. Averaged and offset corrected Raman spectra of SU-8 2050 and SU-8 2075.

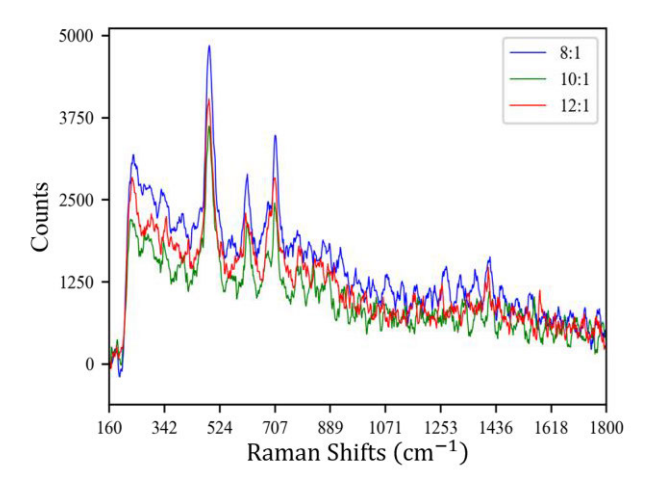


Fig. 5. Averaged and offset corrected Raman spectra of three PDMS mixtures: 8:1, 10:1, and 12:1.

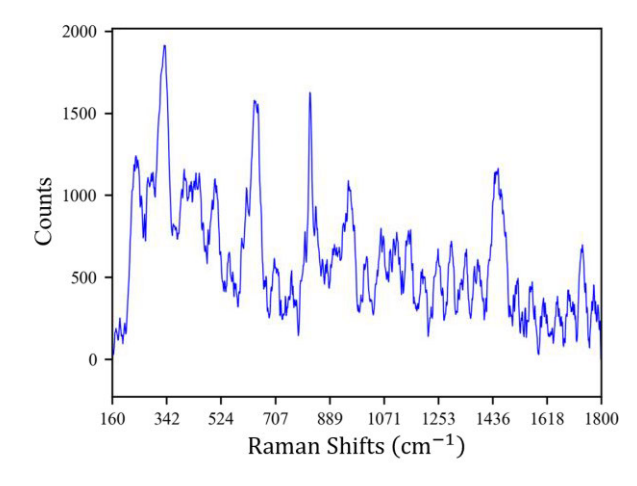


Fig. 6. Averaged and offset corrected Raman spectra of SU-8 developer in the HDPE jar.

averaged spectra are shown in Fig. 6. The main characteristic peaks are at 1466, 821, and 616 cm⁻¹.

Accounting for the accuracy and condition of the gold slides is important for ensuring that the neural network is

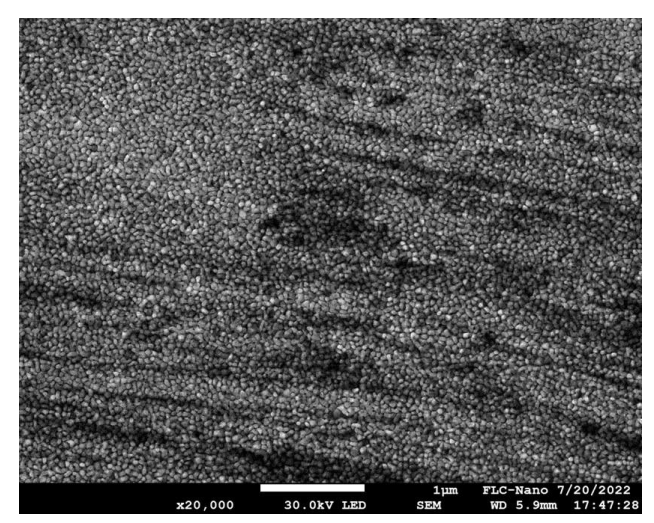


Fig. 7. Scanning electron microscope surface images of a used gold-coated microscope slide.

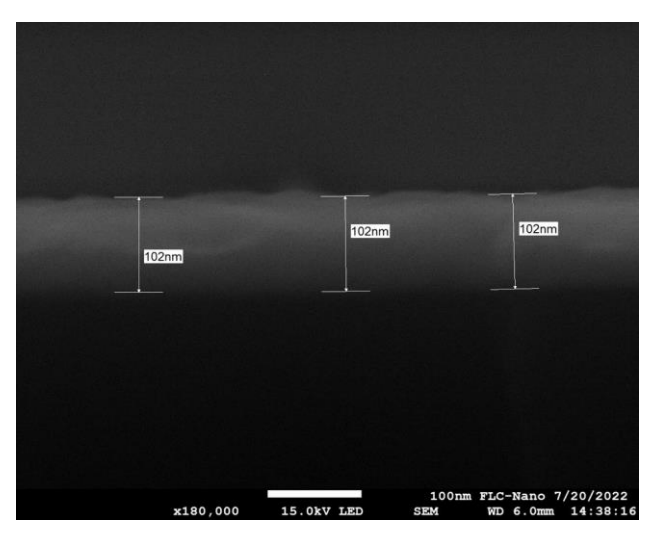


Fig. 8. Scanning electron microscope cross-sectional images of a used gold-coated microscope slide.

identifying differences in the PDMS and not just differences in the gold coating. Scanning electron microscopy was used to characterize the gold-coated microscope slides. The surface of a used microscope slide is shown in Fig. 7. Damage to the gold coating, likely caused during cleaning, is indicated by the dark lines and pits. A cross-sectional image of the gold coating is shown in Fig. 8. The thickness measurements shown in the image verify the thickness reported by the manufacturer.

The neural network was then trained on the dataset. The spectra were labeled as their respective material, regardless of the container. The average accuracy was 100%, and the average runtime was 80.08 s. The performance of the model versus the number of epochs is shown in Fig. 9. These data show that fine-tuning accuracy and loss are relatively unaffected by the number of epochs. However, the pretraining accuracy and loss are affected. To minimize loss and optimize accuracy, at least 20 epochs are required for pretraining. The number of epochs was set to 30 to minimize the pretraining loss. The learning rate was adopted from the paper by

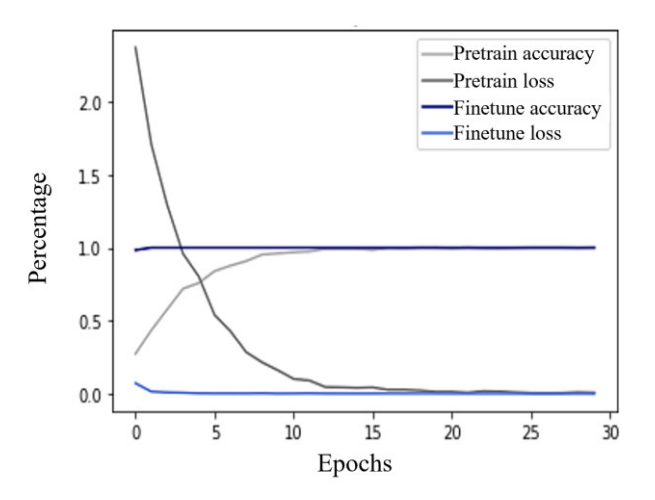


Fig. 9. Model performance versus number of epochs.

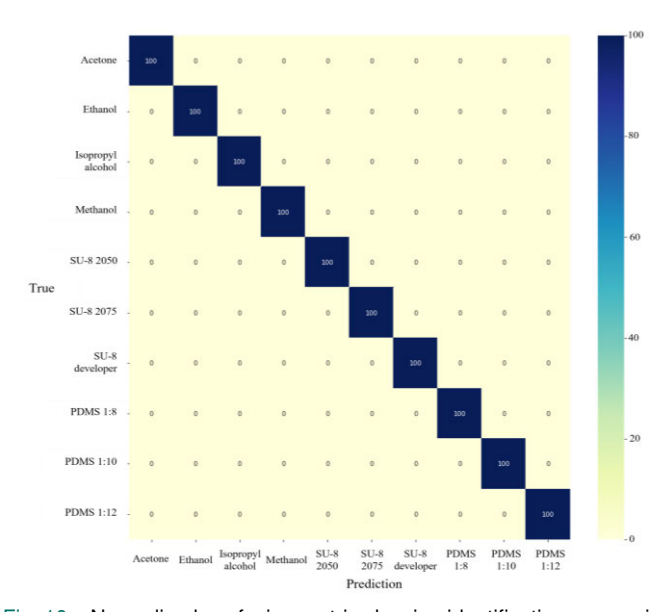


Fig. 10. Normalized confusion matrix showing identification accuracies for the substances.

Kukula et al. [15] and was not optimized further. The model was deemed an adequate fit since the accuracy and loss shown in Fig. 7 do not diverge within the tested number of epochs. The confusion matrix used to visualize the accuracy of the testing network is shown in Fig. 10. The y-axis of the figure shows the true sample, and the x-axis shows the predicted sample. The number and color on the tiles are determined by how many times a sample was predicted to be the same sample or a different sample. The model performed with no error, so the incorrect tiles are labeled with zeros and the color associated with zero errors. The same network had been previously trained using spectra whose characteristic peaks were significantly less intense. The model had less accuracy for these data, so the laser power and the integration time were increased. The performance of the model was deemed adequate although it is likely that the laser power, integration time, and a number of epochs could be further optimized to minimize the acquisition and identification times.

IV. DISCUSSION

In this study, nanofabrication chemicals were identified using Raman spectroscopy and neural networks. Misidentifying laboratory chemicals can be inconvenient and potentially dangerous. Under optimal conditions, substances can be identified based on the characteristic Raman peaks. However, typical storage containers attenuate the Raman spectra making traditional identification methods unreliable. Neural networks can overcome this issue by using models that account for a wide range of conditions.

The first experiment identified four common solvents inside various containers. This allowed for the development of a model that can identify these chemicals when many of the characteristic peaks are significantly attenuated. Averaging the spectra removed most of the random noise and corrected for lower intensity spectra, making the characteristic peaks more distinguishable. The main characteristic peak for each solvent is present in the spectra from all bottles: 798 cm⁻¹ for acetone, 883 cm⁻¹ for ethanol, 820 cm⁻¹ for isopropyl alcohol, and 1035 cm⁻¹ for methanol. Other characteristic peaks are difficult to identify in spectra from amber glass bottles and are often indistinguishable from background noise in spectra from HDPE bottles. Increasing the laser power and integration time would help distinguish the characteristic peaks, possibly making it feasible to identify the weaker spectra without a neural network. However, collecting and averaging 50 spectra without increasing integration time or changing the location of the container could take as long as 15 min, and the results might not be as reliable. Another consideration is that the container and sample may be damaged if the integration time and laser power were increased. The neural network accurately identified all solvents using only one spectrum, with the sample measurement and identification time being completed in under 2 min.

The last experiment differentiated varieties of the same substances: two viscosities of SU-8 photoresist and samples of three cured PDMS ratios. Despite having similar levels of background fluorescence, the characteristic peaks of SU-8 2075 were significantly stronger than the characteristic peaks of SU-8 2050. The spectra of the two SU-8 viscosities were differentiated based on overall intensity but contained the same characteristic peaks. The neural network is not needed for differentiating these two viscosities but would be useful for viscosities that have similar intensities and are otherwise indistinguishable. The spectra of the PDMS

samples had the same characteristic peaks but with slightly different intensities. Unlike the two SU-8 viscosities, the PDMS spectra are indistinguishable based on characteristic peaks. While the characteristic peaks of the PDMS spectra are easily differentiated from the other chemicals, they are nearly indistinguishable from each other.

REFERENCES

- R. S. Das and Y. K. Agrawal, "Raman spectroscopy: Recent advancements, techniques and applications," *Vibrat. Spectrosc.*, vol. 57, no. 2, pp. 163–176, 2011.
- [2] I. De Wolf, C. Jian, and W. M. van Spengen, "The investigation of microsystems using Raman spectroscopy," *Opt. Lasers Eng.*, vol. 36, no. 2, pp. 213–223, Aug. 2001.
- [3] T. Suzuki et al., "Thermal and optical properties of sol-gel and SU-8 resists," *Proc. SPIE*, vol. 8249, pp. 93–101, Feb. 2012.
- [4] G. Persichetti and R. Bernini, "Water monitoring by optofluidic Raman spectroscopy for in situ applications," *Talanta*, vol. 155, pp. 145–152, Aug. 2016.
- [5] T. T. X. Ong, E. W. Blanch, and O. A. H. Jones, "Surface enhanced Raman spectroscopy in environmental analysis, monitoring and assessment," Sci. Total Environ., vol. 720, Jun. 2020, Art. no. 137601.
- [6] M. L. Ramirez-Cedeno, W. Ortiz-Rivera, L. C. Pacheco-Londono, and S. P. Hernandez-Rivera, "Remote detection of hazardous liquids concealed in glass and plastic containers," *IEEE Sensors J.*, vol. 10, no. 3, pp. 693–698, Mar. 2010.
- [7] B. Zachhuber, G. Ramer, A. Hobro, E. T. H. Chrysostom, and B. Lendl, "Stand-off Raman spectroscopy: A powerful technique for qualitative and quantitative analysis of inorganic and organic compounds including explosives," *Anal. Bioanal. Chem.*, vol. 400, no. 8, pp. 2439–2447, Jun. 2011.
- [8] C.-S. Ho et al., "Rapid identification of pathogenic bacteria using Raman spectroscopy and deep learning," *Nature Commun.*, vol. 10, no. 1, pp. 1–8, 2019.
- [9] M. Varnasseri et al., "Portable through bottle SORS for the authentication of extra virgin olive oil," *Appl. Sci.*, vol. 11, no. 18, p. 8347, Sep. 2021.
- [10] B. J. Visser et al., "The diagnostic accuracy of the hand-held Raman spectrometer for the identification of anti-malarial drugs," *Malaria J.*, vol. 15, no. 1, pp. 1–12, Dec. 2016.
- [11] F. Lussier, V. Thibault, B. Charron, G. Q. Wallace, and J.-F. Masson, "Deep learning and artificial intelligence methods for Raman and surface-enhanced Raman scattering," *TrAC Trends Anal. Chem.*, vol. 124, Mar. 2020, Art. no. 115796.
- [12] S. Weng et al., "Deep learning networks for the recognition and quantitation of surface-enhanced Raman spectroscopy," *Analyst*, vol. 145, no. 14, pp. 4827–4835, 2020.
- [13] K. Hennessy, M. G. Madden, J. Conroy, and A. G. Ryder, "An improved genetic programming technique for the classification of Raman spectra," in *Proc. Int. Conf. Innov. Techn. Appl. Artif. Intell.*, 2005, pp. 181–192.
- [14] X. Fan, W. Ming, H. Zeng, Z. Zhang, and H. Lu, "Deep learning-based component identification for the Raman spectra of mixtures," *Analyst*, vol. 144, no. 5, pp. 1789–1798, 2019.
- [15] K. Kukula et al., "Rapid detection of bacteria using Raman spectroscopy and deep learning," in *Proc. IEEE 11th Annu. Comput. Commun.* Workshop Conf. (CCWC), Jan. 2021, pp. 796–799.